^{89}Y-Static and -MAS NMR, and ^{27}Al-MAS NMR in Green Phosphor, Tb-Doped $Y_3Al_5O_{12}$ and Luminous Characteristics

Toshie Harazono,* Etsuzo Yokota, Hiroshi Uchida, and Tokuko Watanabe†

Research Center, Mitsubishi Chemical Co., Ltd., 1000, Kamoshida, Aoba-ku, Yokohama 227-8502

†Tokyo University of Fisheries, 4-5-7, Konan, Minato-ku, Tokyo 108-8477

(Received May 25, 1998)

Luminous properties of a green phosphor, Tb-doped $Y_3Al_5O_{12}$, have been studied by ^{89}Y (nuclear spin 1/2)-static and -magic angle spinning (MAS) NMR and ^{27}Al (nuclear spin 5/2)-MAS NMR. In pure $Y_3Al_5O_{12}$, a sharp signal at 239 ppm was observed in ^{89}Y-MAS NMR spectrum, which was expected from a powder pattern due to 8O-coordinated Y in D_2 symmetry in ^{89}Y-static NMR spectrum. In the ^{27}Al-MAS NMR spectrum of $Y_3Al_5O_{12}$, two typical signals were observed, i.e., a sharp signal at 0 ppm due to 6O-coordinated Al in the octahedral site and a characteristic signal due to 4O-coordinated Al in the tetrahedral site. These ^{89}Y and ^{27}Al signals became broader in Tb-$Y_3Al_5O_{12}$ with increasing in content of the doped Tb. In addition to the main peak at 239 ppm, furthermore, extra peaks appeared in the bottom of the main peak in ^{89}Y-MAS NMR; these were assigned to the second nearest to the fifth nearest neighboring Y (Y^2 to Y^5) atoms to Tb atom substituted in the site of Y atom. Shifts of these Y atoms were reasonably explained by a pseudocontact shift via a paramagnetic Tb^{3+} ion. Incorporation of Tb^{3+} ions caused a large reduction in ^{89}Y nuclear spin-lattice relaxation time from 4000s (pure $Y_3Al_5O_{12}$) to several hundred seconds (3% Tb-$Y_3Al_5O_{12}$) as well.

The line-broadening of the signals was mainly dominated by the dipole–dipole interaction mechanism between the Al or Y resonating nucleus and a Tb^{3+} ion. The signals of Y atoms in the sites where either one of the nearest neighboring Y^1 atoms was replaced by Tb atom were not detected because of the large line-broadening.

The stronger brightness was obtained in the specimens which showed the much broader linewidth in ^{27}Al-MAS signals and in ^{89}Y-static NMR signals under the same Tb content. So we concluded that the homogeneous distribution of Tb^{3+} ions in Tb-$Y_3Al_5O_{12}$ plays a key role for the higher brightness in the green phosphor as in the red phosphor.

Green phosphor, Tb-$Y_3Al_5O_{12}$ (Tb-doped $Y_3Al_5O_{12}$), has been used in a projection cathode-ray tube. Industry strongly desires the phosphor to be prepared in much smaller particles and have higher brightness because televisions tend to become larger. We hope to prepare the phosphor that can realize the high brightness and the high resolution without further increase of incident beam power. In order to develop the phosphor with such characteristics, the crystal field and/or the structure of the emission center must be elucidated with relation to the brightness.

We investigated the details concerning the relationship between the brightness and the Eu distribution in the Eu-Y_2O_3 red phosphor by using ^{89}Y-static NMR, as well as the relationship between the brightness and the defects by ESR.[1] The brightness of the red phosphor is attributable to the homogeneous distribution of Eu atoms in Y_2O_3, not to the paramagnetic lattice defects, according to the facts that Eu-Y_2O_3 phosphors with the same Eu content and with the higher brightness showed broader linewidth of the ^{89}Y signal due to the dipolar interaction to the second neighboring paramagnetic Eu ions, and the paramagnetic lattice defects had no relation to the brightness.

In this paper, we will discuss a distribution of Tb^{3+} ion in Tb-$Y_3Al_5O_{12}$ and its paramagnetic effects to the chemical shift, the spin-lattice relaxation time, and the line-broadening in the ^{89}Y-static and -MAS NMR and ^{27}Al-MAS NMR spectroscopies with the relation to the characteristics of emission efficiency. This paper points out the usefulness of the solid state ^{89}Y-NMR in characterization of the phosphor including Y atom, although only few studies[1—10] via ^{89}Y-NMR (nuclear spin = 1/2 and natural abundance 100%) has been done because of its low resonance frequency, 14.706 MHz at 7.05 T, low sensitivity (1.18×10^{-4} times to ^{1}H), and long spin-lattice relaxation times (several hours[2]).

Experimental

Materials: All the samples used in this study are listed in Table 1. The raw materials, Y_2O_3 and Tb_4O_3, were prepared by Mitsubishi Chemical Co., Ltd., and the other materials were purchased from Wako Co., Ltd., Junsei Co., Ltd., and Kanto Chemical Co., Ltd. The raw materials, Y_2O_3, Tb_4O_3, and Al_2O_3, were luminescence grade and all other purchased materials were reagent grade.

The samples in this experiment were prepared by the method described in the handbook of phosphors[11] and a patent.[12] The preparation procedures are as follows. *$Y_3Al_5O_{12}$ (= MG1) and Tb-doped $Y_3Al_5O_{12}$ (= MG2 to MG6)*: BaF_2 was added to raw materials, Y_2O_3, Tb_4O_3 (except in MG1) and Al_2O_3 as the flux in an alumina crucible and the mixture was heated to 1470 °C and held for several hours to produce Tb-doped $Y_3Al_5O_{12}$ (Tb-$Y_3Al_5O_{12}$). *Tb-doped $Y_3Al_5O_{12}$ (= MG7)*: Raw materials, Y_2O_3,

Table 1. Sample List and the Spin-Lattice Relaxation Times (T_1) of the Main Peaks at 239 ppm in ^{89}Y-MAS Spectra of Pure and Tb-Doped $Y_3Al_5O_{12}$

Sample	$(Y_cTb_{1-c})_3Al_5O_{12}$		Chroma	Particle size	Brightness	T_1[1] [b)]
	c	$1-c$ [a)]	x/y [24)]	$d_{50}/\mu m$	%	s
MG1	1.00	0.00	0.504/0.444	4.40	—	3950
MG2	0.99	0.01	0.309/0.434	4.44	49	3140
MG3	0.98	0.02	0.328/0.488	4.20	59	1160
MG4	0.97	0.03	0.335/0.506	4.20	73	560
MG5	0.95	0.05	0.341/0.523	4.21	74	
MG6	0.90	0.10	0.351/0.534	4.22	73	
MG7	0.95	0.05	0.348/0.528	4.32	100	

a) Activator content. b) T_1 of peaks at 239 ppm were measured by the saturation recovery method. The peak intensities were fitted by the function of $I = I_0^{\,l}\{1-\exp(-\tau/T_1^{\,l}\}+I_0^{\,s}\{1-\exp(-\tau/T_1^{\,s})\}$, where I_0 is constant and τ is waiting time, by employing the non-linear least square method with two components, long (l) and short (s) components. The short components were about several ten seconds for MG2 to MG4. The rate of the short component for MG1 is nealy zero.

Tb_4O_3, and Al_2O_3 were mixed with pure water and dried at 120 °C for 5 h. Continuously, BaF_2 was added to the dried powder as the flux. By heating the mixture in an alumina crucible to 1470 °C, a co-precipitation Tb-$Y_3Al_5O_{12}$ was produced. All the obtained Tb-$Y_3Al_5O_{12}$ materials were washed with pure water several times and dried. Hereafter, we use notation, MGi (i = 1 to 7) as the sample name. The Tb content in each sample is tabulated in Table 1 together with other properties, such as chroma, particle size and brightness.

Apparatus and Measurements: Each molar ratio, Tb/Y, and the amounts of impurity were determined by Seiko SPS-1200A ICP and Rigaku 3370 fluorescence X-ray spectrometers. The amounts of impurities of all samples were less than 1 ppm. The activator content was consistent with the analytical concentration of Tb within the experimental error. The crystal structure of Tb-$Y_3Al_5O_{12}$ was identified in powder by an X-ray diffractometer with monochromated Cu Kα (Philips PW1700 diffractometer). The emission spectra and the intensities of brightness were measured with a TOPCON ABT-32 electron-ray emission spectrometer. The particle size was measured with a Model PA-2 Coulter Counter. ^{89}Y-MAS and -static NMR measurements were carried out at 14.706 MHz on a Bruker MSL-300 spectrometer equipped with a 7 mm low-frequency CP (cross polarization)-MAS probe (dia. 7 mm) at a spinning rate of 5 kHz and a static probe (dia. 10 mm), respectively. The measurements of ^{27}Al-MAS NMR spectrum were carried out at 78.205 MHz on a Bruker MSL-300 spectrometer equipped with a 4 mm probe (dia. 4 mm) at a spinning rate of 15 kHz. Chemical shifts were determined relatively to 1.5 M $Y(NO_3)_3$ and 1.5 M $Al(NO_3)_3$ aqueous solutions as 0 ppm for ^{89}Y and ^{27}Al NMR, respectively. A 90 ° pulse width was 20 μs (static probe) and 11 μs (MAS probe) for ^{89}Y in 1.5 M $Y(NO_3)_3$ aqueous solution and 3 μs (MAS probe) for ^{27}Al in 1.5 M $Al(NO_3)_3$ aqueous solution. The 0.6 μs pulse was used for ^{27}Al-MAS NMR measurement. A single pulse was used for MAS and static measurements. All measurements were performed at room temperature.

Results

Crystal Structure of $Y_3Al_5O_{12}$ and Tb-$Y_3Al_5O_{12}$: The schematic diagram of crystal structure[13] for $Y_3Al_5O_{12}$ is shown in Fig. 1a. In a unit cell, 24 Al atoms at the tetrahedral site (Al(4), 4O atoms-coordinated Al), 16 Al atoms at the octahedral site (Al(6), 6O atoms-coordinated Al), 24 Y atoms

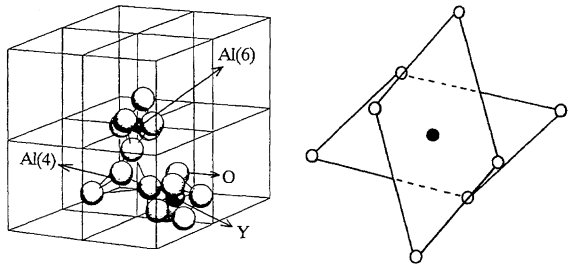

Fig. 1. (a) Schematic crystal structure of $Y_3Al_5O_{12}$. Al-(4) and Al(6) express as the 4O-coordinated Al and 6O-coordinated Al, respectively. (b): Coordination scheme around Y atom. ●: Y and ○: O.

at the dodecahedral site (8O atoms-coordinated Y), and 96 O atoms exist. Hereafter, the central Y atom is named as Y^0, the first nearest neighboring Y atom through O atom as Y^1 (i.e., Y^0–O–Y^1), the second nearest neighboring Y atom through O atoms as Y^2 (i.e., Y^0–O–Al(6) or Al(4)–O–Y^2) and the third or further far neighboring Y atom as Y^n ($n \geq 3$). If Tb is substituted for Y, Tb becomes Tb^0 and other atoms are named in the same manner. In Fig. 1b the local coordination geometry around the Y atom (Y^0) is illustrated. The X-ray powder diffraction patterns of Tb-$Y_3Al_5O_{12}$ were almost the same for that of the pure $Y_3Al_5O_{12}$ up to 10 mol% content of Tb. The emission patterns of all Tb-$Y_3Al_5O_{12}$ showed a peak at 543.5 nm.[14]

^{89}Y-Static and -MAS NMR Spectra: As shown in Fig. 2a, the ^{89}Y-static NMR spectrum of $Y_3Al_5O_{12}$ with D_2 symmetry of Y shows the characteristic powder pattern of nearly axial symmetry (σ_{11} = 306 ppm, σ_{22}—σ_{33} = 203 ppm). The isotropic chemical shifts, σ_{iso} (static) calculated from $(\sigma_{11}+\sigma_{22}+\sigma_{33})/3$ = 237 ppm, is in good agreement with the σ_{iso}(MAS) = 239 ppm (Fig. 2b) within the experimental error. The ^{89}Y-static spectra of Tb-$Y_3Al_5O_{12}$ (MG2 to MG5) and ^{89}Y-MAS spectra of Tb-$Y_3Al_5O_{12}$ (MG2 to MG6) were depicted in Figs. 3a and 3b, respectively, together with those of pure $Y_3Al_5O_{12}$ (MG1) for a comparison. The ^{89}Y-static NMR spectra showed the maximum intensity at the nearly

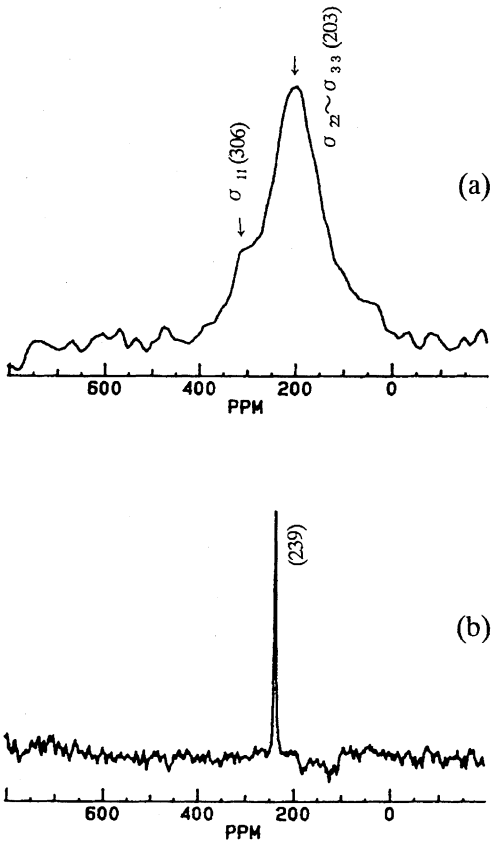

Fig. 2. ^{89}Y-solid state NMR spectra of pure $Y_3Al_5O_{12}$. (a): static; (Spectral width: 50000 Hz, data point: 4 K, pulse width: 7 μs, aquisition number: 159 times, recycle time: 1000 s, dead time: 100 μs). (b): MAS; (Spectral width: 15000 Hz, data point: 4 K, pulse width: 11 μs, aquisition number: 23 times, recycle time: 1000 s, spinning rate: 5000 rps, dead time: 150 μs).

constant field, 203 ppm (corresponding to σ_{22}—σ_{33}) and the line-broadening of the signal with increasing in Tb content. No signal of MG6 or MG7 was detected in the static NMR because their line-broadening was too massive. In MAS NMR spectra, several shoulder peaks appeared additionally in the bottom of the central peak. These peaks became more conspicuous with Tb content. At about 80 ppm an extra peak appeared and its intensity became larger with Tb content.

^{27}Al-MAS NMR Spectra: Figure 4 demonstrates the ^{27}Al-MAS NMR spectra of pure $Y_3Al_5O_{12}$ (MG1) and Tb-$Y_3Al_5O_{12}$ with 1 to 10 mol% Tb content (MG2 to MG7). Pure $Y_3Al_5O_{12}$ showed two signals, one at 0 ppm and the other spreading between 20 and 60 ppm. The former was assigned to 6O-coordinated Al, (Al(6)) in the octahedral site and the latter to 4O-coordinated Al, (Al(4)) in the tetrahedral site.[15] The ^{27}Al spectra for MG2 to MG7 were deconvoluted to each signal for Al(6) and Al(4) on the assumption that each signal is symmetrical. The assumption was based on the report on the symmetrical pattern for Al(6) ($1/2 \longleftrightarrow -1/2$) and Al(4) ($1/2 \longleftrightarrow -1/2$) transitions in $Y_3Al_5O_{12}$.[15] The signal position was determined at the peak point for Al(6) signal and at the axis of symmetry for Al(4) signal.

Spin-Lattice Relaxation Times of ^{89}Y Resonance: Saturation recovery curves of the main peak (239 ppm) in pure $Y_3Al_5O_{12}$ and Tb-$Y_3Al_5O_{12}$ were analyzed by employing the bi-exponential non-linear least square curve fitting, because mono-exponential analysis could not reproduce the recovery curves except pure $Y_3Al_5O_{12}$. Only one Y species was recognized in pure $Y_3Al_5O_{12}$ (MG1) from the view point of T_1, i.e., T_1 of which was 3950 s and very long. On the other hand, at least two species with different T_1 value were recognized in Tb-$Y_3Al_5O_{12}$. As shown in Table 1, the longer T_1 value in Tb-$Y_3Al_5O_{12}$ was gradually reduced from Ca. 4000 s for MG1 to 560 s for MG4 with increasing in the Tb content. The shorter T_1 distributed in the range from 60 to 10 s and had no relation to the Tb content.

The T_1 value of a shoulder peak around 210 ppm, which was selected as an example of the shoulder peaks appearing with Tb doping, was also analyzed in the same manner for convenience. Saturation recovery curves at 210 ppm peak showed at least two T_1 values; one is several dozen seconds with 50—60% of population and the other is several hundred seconds. T_1 of the former component is in the same order with T_1 of the shorter component in the main peak, suggesting the existence of species affected by the paramagnetic Tb^{3+} ion. T_1 of the latter component is close to the longer component of the main peak, suggesting an overlap of the tail of the longer component of the main peak and/or Y species with less effect via Tb^{3+} ion.

The T_1 value of the extra signal at about 80 ppm was in the range of 100 s to several hundreds of seconds as a result of the single exponential analysis, and was found in the range of 80 to 200 s as the shorter component and several hundreds of seconds as the longer component by the bi-exponential analysis. As the recycle time for ^{89}Y-NMR measurements was set between 1000 s and 240 s for MAS NMR (Fig. 3b) and 10 s for static NMR (Fig. 3a), signals from nuclei with long spin-lattice relaxation times are saturated and the relative intensities of signals with short spin-lattice relaxation times increase.

Discussion

Assignment of the ^{89}Y-MAS NMR Signals via the Pseudocontact Shift: When Tb atoms were doped in $Y_3Al_5O_{12}$, the central peak position of the ^{89}Y-MAS signals was kept constant at the position of the pure $Y_3Al_5O_{12}$ (239 ppm), but the line-shapes gradually changed with additional shoulder peaks (Fig. 3b). Since the incorporation of paramagnetic Tb^{3+} ions did not cause any shift in the ^{89}Y signal at 239 ppm, this signal is assigned to $Y^n(-O-X)_{n-1}-O-Tb$ (X = Al(4), Al(6) or Y) where Y^n is far apart from Tb (as discussed later, $n \geq 6$). Hereafter we call such a Y^n atom which is nearly free from Tb effect as a diamagnetic Y atom. On the other hand, the shoulder peaks become visible with increasing in the Tb content in Tb-$Y_3Al_5O_{12}$. Therefore, these shoulder peaks must results from Y in the crystallite containing paramagnetic ions, the shifts of which are caused by a contact and/or a pseudocontact mechanism via Tb^{3+} ions. As shown in Tables 2, 3, and 4, about fifty Y atoms locate within 1 nm

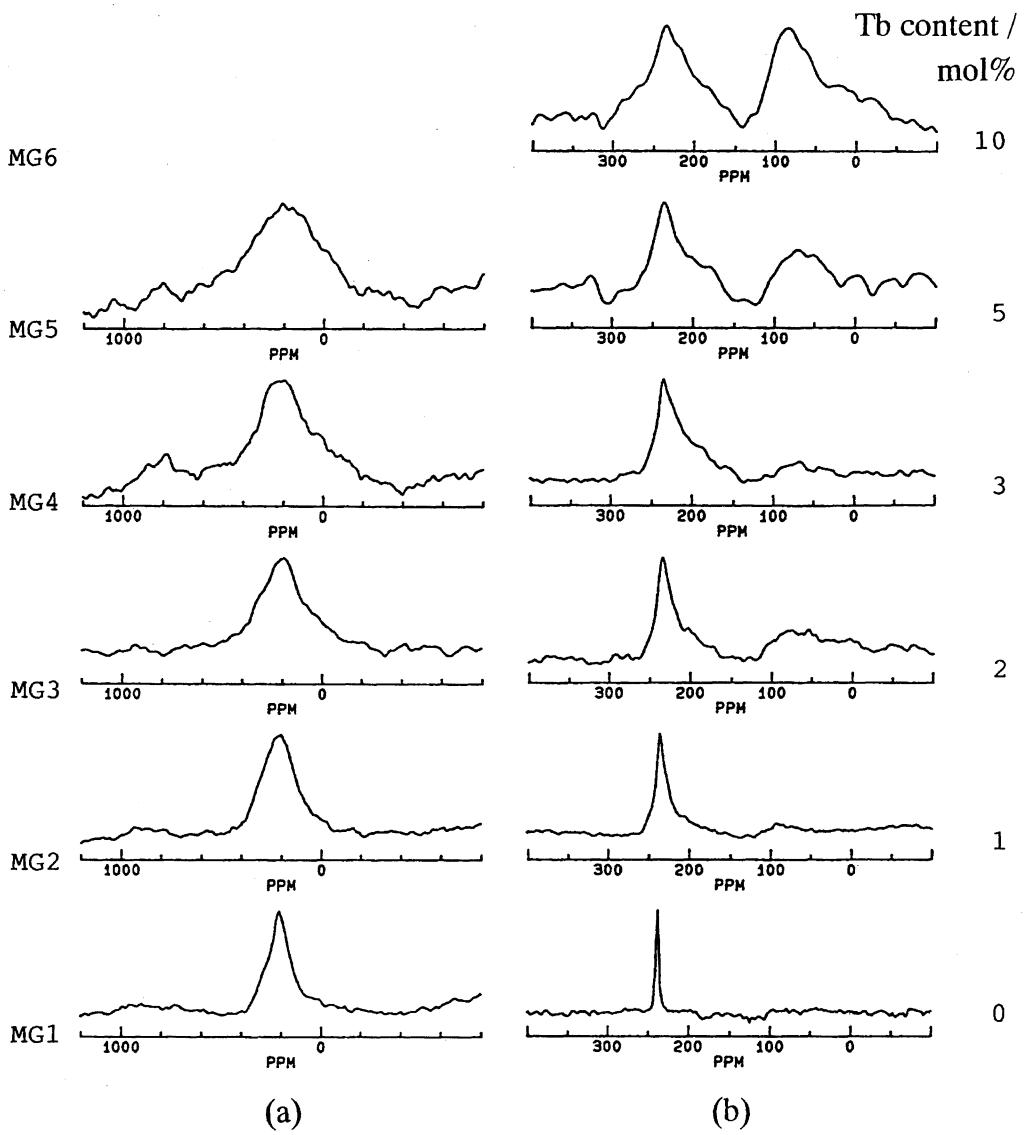

Fig. 3. ^{89}Y-solid NMR spectra of the pure and Tb-doped $Y_3Al_5O_{12}$. (a): Static NMR spectra of MG1 to MG5. (Spectral width: 200000 Hz, data point: 8 K, 90° pulse: 20 μs, pulse width: 5 μs, aquisition number: 3300—17000, recycle time: 10 s, dead time: 50 μs). (b): MAS NMR spectra of MG1 to MG6. (Spectral width: 30000 Hz, data point: 4 K, 90° pulse: 11 μs, pulse width: 7 μs, aquisition number: 200 to 250 times, recycle time: MG1; 1000 s, MG2; 400 s, MG3; 750 s, MG4; 320 s, MG5; 280 s, MG6; 240 s, spinning rate: 5000 rps, dead time: 150 μs).

of Y^0, Al(6), and Al(4) atoms in $Y_3Al_5O_{12}$, respectively.[16] Tb atoms replace mostly at the sites of Y atoms in the same manner as in the case of Er atoms in $(Er_xY_{1-x})Al_5O_{12}$.[17]

The pseudocontact contribution to the shift of Y^1 to Y^n resonance via Tb^{3+} ions which replace Y^0 was estimated as follows; the net pseudocontact shift ΔH_p for a paramagnetic ion in axial symmetry is given by

$$\Delta H_p = (-g^2\beta^2 J(J+1)(2J-1)(2J+3)A_2^0\langle r^2\rangle(3\cos^2\theta - 1) \times \langle J//\alpha//J\rangle H_0)/(60(kT)^2 r^3),$$

where g is the Lande g factor, J the quantum number of a total angular momentum of the paramagnetic ion, $A_2^0\langle r^2\rangle$ a crystal field parameter, r the Tb^{3+}–Y distance, θ the angle between the principal magnetic axis through Al(4)–Tb^{3+}(Y)–Al(4) at Tb^{3+} and the Tb^{3+}–Y vector, and $\langle J//\alpha//J\rangle$ a numerical coefficient.[18] In this equation a contribution from the structural term, $(3\cos^2\theta - 1)/r^3$, is calculated from the crystal structure data. In order to estimate a contribution from the other term, $(-g^2\beta^2 J(J+1)(2J-1)(2J+3)A_2^0\langle r^2\rangle\langle J//\alpha//J\rangle H_0)$, we utilized the shift observed in ^{89}Y-MAS NMR of Eu-Y_2O_2S.[19] The peaks of Y^1(–O–, –O–)Eu and Y^1(–O–, –S–)-Eu shifted to +75.5 ppm (lower field) and −61.0 ppm (higher field) from the main peak, respectively, mainly through the pseudocontact mechanism. Taking off the contribution via the structural term by substituting r and θ for Y^1–Eu in Table 5, the contribution via the other terms became 3.61 on the average. If we consider the difference of an effective magnetic moment between Tb^{3+} ($4f^8$, 9.5 μ_β) and Eu^{3+} ($4f^6$, 3.4 μ_β),[20] the contribution from the other terms via Tb^{3+} should became 2.8 (= $\mu(Tb^{3+})/\mu(Eu^{3+})$) times larger than that via Eu^{3+} under the assumption that $A_2^0\langle r^2\rangle$ equals in

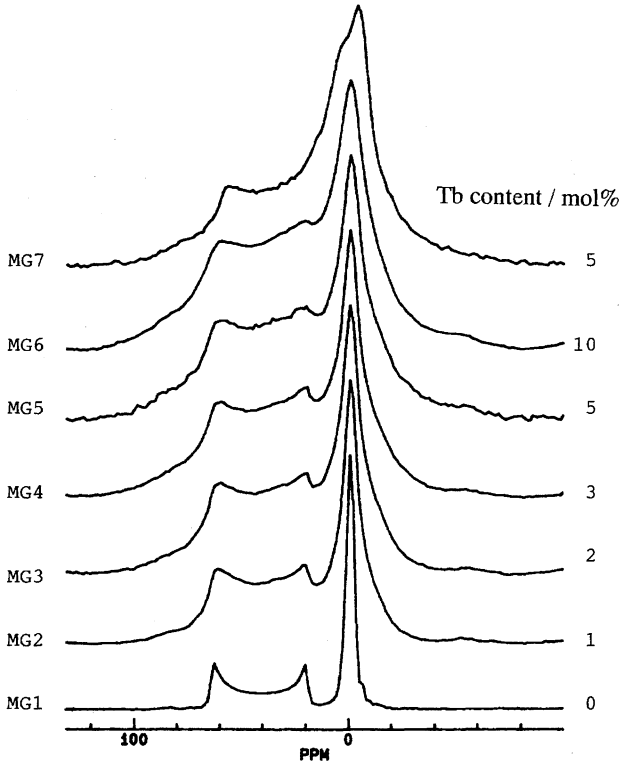

Fig. 4. ^{27}Al-MAS NMR spectra of MK1 to MK7. (Spectral width: 500000 Hz, data point: 8 K, 90° pulse of ^{27}Al in aqueous $Al(NO_3)_3$ solution: 3.1 μs, pulse width: 0.6 μs, aquisition number: 450—29000, recycle time: 2 s, dead time: 2 μs).

the both cases of Eu-Y_2O_2S and Tb-$Y_3Al_5O_{12}$. Therefore, the net pseudocontact contribution to the shift for Y^1 to Y^5 resonance is estimated as listed in Table 5. The estimated position and its intensity for Y^1 to Y^5 resonance was depicted by the line in Fig. 5 together with the observed ^{89}Y-MAS NMR spectrum for MG6. The correlation between the observed shoulder peaks and the expected positions is rather good, except at −102 ppm for Y^1–O–Tb. If the value of $A_2^0\langle r^2\rangle$ for Tb–$Y_3Al_5O_{12}$ is corrected more precisely, the fitting will be better. The contribution from Y^n (n = or > 6) is expected on calculation to add several peaks with very small pseudocontact shifts (less than 10 ppm) in the central

Table 2. The Kinds and Numbers of Atoms around $\underline{Y^0}$ Atom and the Distances from $\underline{Y^0}$

Shell No.	Kind of atom	Distance from Y^0 / Å	Number	Bond
0	$\underline{Y^0}$	0	1	$\underline{Y^0}$
1,2	O	2.302	4	
3,4	O	2.438	4	
5	Al(4)	3.002	2	$\underline{Y^0}$–O–Al(4)
6	Al(6)	3.356	4	$\underline{Y^0}$–O–Al(6)
7	Y^1	3.677	4	$\underline{Y^0}$–O–Y^1
7	Al(4)	3.677	4	$\underline{Y^0}$–O–Al(4)
24	Y^2	5.616	8	$\underline{Y^0}$–O–X–O–Y^2
29	Y^2	6.004	2	$\underline{Y^0}$–O–X–O–Y^2
41	Y^3	6.713	8	$\underline{Y^0}$(–O–X)$_2$–O–Y^3
53	Y^3	7.040	4	$\underline{Y^0}$(–O–X)$_2$–O–Y^3
76	Y^4	8.221	8	$\underline{Y^0}$(–O–X)$_3$–O–Y^4
83	Y^4	8.491	4	$\underline{Y^0}$(–O–X)$_3$–O–Y^4
117	Y^5	9.253	12	$\underline{Y^0}$(–O–X)$_4$–O–Y^5

X = Y, Al(4), Al(6).

part of the signal, but these peaks are overlapping the main peak and become indistinguishable. Therefore, the shoulder peaks spreading to the both sides of the bottom of the main peak are mainly assigned to Y^2, Y^3, Y^4, and Y^5 atoms. This assignment is strengthened by the T_1 value. As mentioned above, T_1 value of the major component at the shoulder peak around 210 ppm was one or two order shorter than T_1 of pure $Y_3Al_5O_{12}$ and of the longer component (mostly diamagnetic Y) of the main peak of Tb-$Y_3Al_5O_{12}$.

The signal for Y^1–O–Tb in Tb-$Y_3Al_5O_{12}$ was not detected at the position estimated by the pseudocontact mechanism. The signal for Y^1–O–Eu in Eu–Y_2O_3, where at least one of 12 nearest neighboring Y atoms to Y^1 was replaced by one Eu atom, appeared at about 200 ppm upper field compared to the main peak for diamagnetic Y(–O–Y, –Y)$_6$.[1] The Y^1–Eu distance is in the range of 3.5—4 Å in Y_2O_3. Considering this result and the difference of the effective magnetic moment between Tb^{3+} and Eu^{3+}, the signal of the Y^1 atom (Y^1–O–Tb) should shift by more than 200 ppm higher field from the main peak, i.e. to nearly 100 ppm. As shown in Fig. 5, there exists one broad signal at 80 ppm, the intensity of which

Table 3. The Kinds and Numbers of Atoms around $\underline{Al(6)}$ Atom and the Distances from $\underline{Al(6)}$

Shell No.	Kind of atom	Distance from Al(6) / Å	Number	Bond
0	$\underline{Al(6)}$	0	1	$\underline{Al(6)}$
1	O	1.919	6	
2	Y^1	3.356	6	$\underline{Al(6)}$–O–Y^1
2	Al(4)	3.356	6	$\underline{Al(6)}$–O–Al(4)
13	Y^2	5.412	6	$\underline{Al(6)}$–O–X–O–Y^2
30	Y^3	6.878	12	$\underline{Al(6)}$(–O–X)$_2$–O–Y^3
43	Y^4	8.083	18	$\underline{Al(6)}$(–O–X)$_3$–O–Y^4
60	Y^5	9.130	6	$\underline{Al(6)}$(–O–X)$_4$–O–Y^5

X = Y, Al(4), Al(6).

Table 4. The Kinds and Numbers of Atoms around Al(4) Atom and the Distances from Al(4)

Shell No.	Kind of atom	Distance from Al(4) / Å	Number	Bond
0	Al(4)	0	1	Al(4)
1-2	O	1.776	4	
3	Y^1	3.002	2	Al(4)–O–Y^1
4-6	O	3.313	4	
7	Al(6)	3.356	4	Al(4)–O–Al(6)
8-11	O	3.639	8	
12	Y^1	3.677	4	Al(4)–O–Y^1
12	Al(4)	3.677	4	Al(4)–O–Al(4)
33	Y^2	5.616	8	Al(4)–O–X–O–Y^2
36	Y^2	6.004	4	Al(4)–O–X–O–Y^2
56	Y^3	7.040	4	Al(4)(–O–X)$_2$–O–Y^3
88	Y^4	8.221	8	Al(6)(–O–X)$_3$–O–Y^4
119	Y^5	9.006	10	Al(6)(–O–X)$_4$–O–Y^5
133	Y^5	9.253	12	Al(6)(–O–X)$_4$–O–Y^5

X = Y, Al(4), Al(6).

Table 5. The Calculated Chemical Shifts of Y^1 to Y^5 for Tb-$Y_3Al_5O_{12}$ and the Observed Chemical Shifts of Y^1 for Eu-Y_2O_2S

Shell No.	Y	r[a] / Å	θ / degree[b]	$(3\cos^2\theta-1)/r^3$ / 10^{21} cm^{-3}	Number of Y atom	Δ[c] / ppm	Chemical shift / ppm[d]
7	Y^1	3.677	65.9	−10.06	4	−102.0	137.0
24	Y^2	5.616	36.7	5.242	4	53.1	292.1
24	Y^2	5.616	74.5	−4.436	4	−45.0	194.0
29	Y^2	6.004	0.0	9.241	2	93.7	332.7
41	Y^3	6.713	63.4	−1.322	8	−13.4	225.6
53	Y^3	7.040	50.2	0.652	4	6.6	245.6
76	Y^4	8.221	79.5	−1.620	4	−16.4	222.6
76	Y^4	8.221	24.1	2.700	4	27.4	266.4
83	Y^4	8.491	90.0	−1.634	4	−16.6	222.4
117	Y^5	9.253	80.7	−1.163	4	−11.8	227.2
117	Y^5	9.253	60.9	−0.365	4	−3.7	235.3
117	Y^5	9.253	35.8	1.228	4	12.4	251.4
Y^1(–O–, –O–)Eu[e]		3.61	37.2	19.2	3	75.5[f]	
Y^1(–O–, –S–)Eu		3.78	90.0	−18.5	6	−61.0	

a) r is the Tb–Y distance. b) θ is the angle between the principal axis through Al(4)–Tb^{3+}(Y)–Al(4) at Tb^{3+} and the Tb^{3+}–Y vector. c) Δ is the calculated paramagnetic shifts of each Y atom for Tb–$Y_3Al_5O_{12}$ on the assumption that the paramagnetic shifts of Y^1 to Y^5 are mainly dominated by the pseudocontact mechanism and from the results that the magnetic moment ratio of Tb/Eu is 2.8. − sign represents the higher field shift and + sign the lower field shift. d) The chemical shift calculated from c). e) Y^1 for Eu–Y_2O_2S, in Ref. 19. f) The observed paramagnetic shifts of Y^1 for Eu–Y_2O_2S.

increases with the Tb content. However, the T_1 of this signal is about one order longer than that of Y^2–O–X–O–Tb. This does not make sense for assignment of the signal at 80 ppm to Y^1–O–Tb. Consequently, the signal for Y^1–O–Tb must have too broad a linewidth to be detected via a paramagnetic Tb^{3+} ion locating at a short distance (3.7 Å). We should pay attention to the fact the growth of the signals at 80 ppm is parallel to that of the shoulder peaks mentioned above with increasing in Tb content and that the T_1 values of both signals are in the same order. This fact might suggest some disorder in the mother lattice, $Y_3Al_5O_{12}$, i.e., appearance of the two magnetically different sites of Y center, by substituting Tb for Y. The origin of the signal at 80 ppm is not clear at the moment.

Distribution of Tb^{3+} Ions: If we assume the completely random (homogeneous) distribution of Tb atoms in the position of Y atoms in $Y_3Al_5O_{12}$, the population of Y^n becomes Tb : Y^1 : Y^2 : Y^3 : Y^4 : Y^5 : diamagnetic Y = 2 : 8 : 20 : 24 : 24 : 22 : 0, that is, the diamagnetic Y atom disappears, when 2% of Y atom were replaced by Tb atom (MG3). Therefore, the sample with less than 2% of Tb such as MG2 includes all types of Y atom and especially high content of the diamagnetic Y, while the sample with higher than 2% of Tb has no diamagnetic Y and includes only Y^1—Y^4

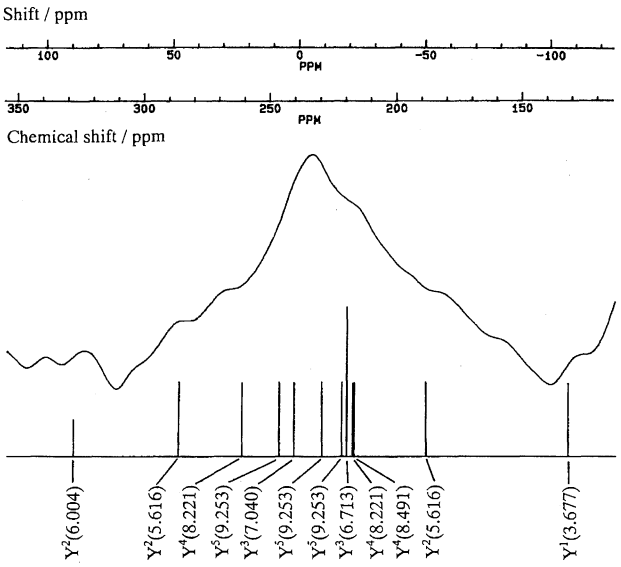

Fig. 5. Assignment of the signals for Y^2 to Y^5 for Tb-$Y_3Al_5O_{12}$. The shifts of Y^2 to Y^5 were calculated on the assumption that these shifts are mainly dominated by the pseudocontact mechanism. The observed ^{89}Y-MAS spectrum for MG6 with the peak top at 235 ppm was indicated. 0 ppm for the shift scale corresponds to the chemical shift of MG1 at 239 ppm.

in MG4, Y^1—Y^3 in MG5, and Y^1—Y^2 in MG6. However, the peak position of the main peak was kept within several ppm and the presence of the diamagnetic Y was experimentally confirmed in Tb-$Y_3Al_5O_{12}$, as shown in Fig. 3b and Table 1. Moreover, the spectrum of MG6 in Fig. 5 showed the coexistence of not only Y^2, but also Y^3 to Y^5 and the diamagnetic Y. Consequently, the assumption of homogeneous distribution of Tb atoms doped in $Y_3Al_5O_{12}$ is never satisfied. Each sample must be composed of crystallites with higher density and with lower density of Tb atoms, as we have already described in the red phosphor, Eu-Y_2O_3.[1)]

Line-Broadening via Paramagnetic Tb^{3+}: The linewidth via dipole–dipole interaction between the Y nuclear spin and the paramagnetic electron spins in Tb^{3+} ion is estimated by the following:[21)]

$$\Delta\nu_{1/2} \propto \sum N_j/r_j^3,$$

where r_j is the distance between Y or Al and Tb, and N_j is the number of Tb at r_j. Using the Tb–Y distance listed in Table 5, the line-broadening of Y^2, Y^3, Y^4, and Y^5 signals is in the ratio of 1 : 0.55 : 0.3 : 0.22, respectively. The Y^2 atoms have more than twice the line-broadening of other Y species. In the crystallite with the high density of Tb^{3+} ion in the homogeneous distribution, a population of Y^1 and Y^2 (i.e., N_1 and N_2) highly increases, which results in a signal loss by Y^1 and in the much broader spectrum-width by Y^2. Furthermore, not only one, but also more than two Tb^{3+} ions can surround one Y, which results in two or more times of broadening, as well as a shift, resulting in signal loss. In the crystallite with the lower density of Tb^{3+} ion, on the other hand, a population of the diamagnetic Y (i.e., for example N_6 and N_7) as well as Y^n with larger n (i.e., for example N_4 and N_5) relatively increases, resulting in a rather narrow signal. Therefore, only Y^2 to Y^5 and the diamagnetic Y atoms distributing randomly (homogeneously) in the crystallite with lower Tb density are detectable in ^{89}Y-NMR.

The line shapes of ^{89}Y-MAS NMR spectra (Fig. 3b) were gradually changed with the Tb content and the higher field shoulder around 220—200 ppm grew up in advance of the other shoulder peaks. As mentioned in Fig. 5, in 220—200 ppm region of the spectrum there exists Y^3 with twice intensity, two Y^4, and Y^5 in the close neighborhood. Since the line-broadening via the paramagnetic Tb ion becomes less as the Y–Tb distance increases, the higher field shoulder at 220—200 ppm is apparently observed in higher intensity than the other part.

Relationship between the Spectrum-Width Broadening of the Signals and the Brightness: Tb^{3+} ions doped in $Y_3Al_5O_{12}$ caused the overall line-broadening of the ^{89}Y and ^{27}Al signals. As discussed above, the observed ^{89}Y spectra for Tb-$Y_3Al_5O_{12}$ do not consist of a single absorption, but of several absorptions with different chemical shifts and possibly chemical shift anisotropies. The spread of the spectrum is in about 82 ppm (1200 Hz) via the Y species with different pseudocontact chemical shifts in the ^{89}Y-MAS NMR spectra (Fig. 5) and in about 102 ppm (1500 Hz) via the chemical shift anisotropy for ^{89}Y-static NMR of pure $Y_3Al_5O_{12}$ (Fig. 2). In comparison with these spreads, the spectral-widths observed in the ^{89}Y-static NMR spectra were extremely large (410 ppm (6000 Hz) in MG5 and more in MG6 and MG7). Therefore, the line-broadening is mainly attributable to the susceptibility effect via incorporated paramagnetic Tb ions.[22)] A net spectrum-width broadening, Δ, in the ^{89}Y-static signals between MGi ($i = 2$—5) and pure $Y_3Al_5O_{12}$ (MG1), i.e., $\Delta = \{\Delta\nu_{1/2}(\mathrm{MG}i) - \Delta\nu_{1/2}(\mathrm{MG1})\}$, was plotted against the Tb content in Fig. 6a, where $\Delta\nu_{1/2}$ was defined as the spectrum-width at the half intensity of the signal. It is interesting that the net spectrum-width broadening showed a good linear correlation to the doped Tb content. According to the empirical observation in Fig. 6a, under the condition that the Tb content is the same, homogeneous distribution of Tb atoms results the larger spectrum-width broadening and the heterogeneous distribution results in the narrower spectrum-width in the ^{89}Y-static NMR spectra.

The same discussion is applicable to the line-broadening of ^{27}Al-MAS signal. The net broadening, Δ, of the spectrum-widths for Al(6) signals were plotted against the Tb content in Fig. 6b. The net broadening of Al(6) signals had a good linear correlation to the Tb content investigated so far.

Compared with the spectrum-width broadenings of ^{89}Y and ^{27}Al signals for MG5 and MG7, in which the Tb content is kept constant at 5 mol% but the preparation method is different each other, MG7 showed larger spectrum-width broadenings for both nuclei than MG5. This means that a larger amount of all the Tb^{3+} ions incorporated are more homogeneously distributed in MG7 than in MG5. As shown in Table 1, the brightness is much higher in MG7 than in MG5. As already pointed out in the previous paper, the

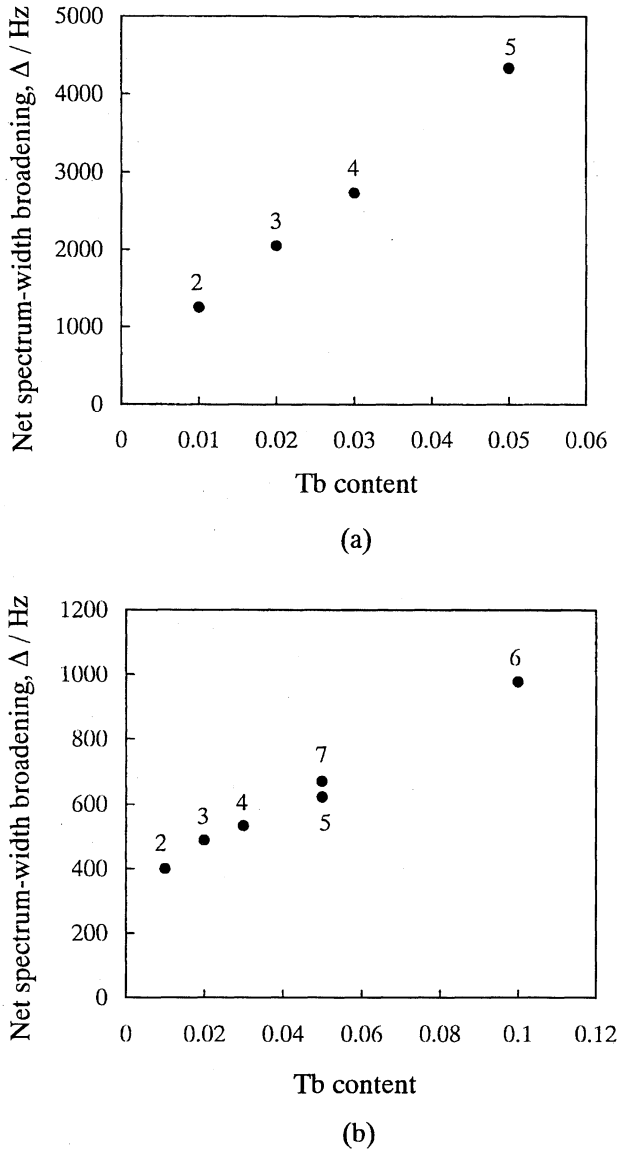

Fig. 6. Plots of the net spectrum-width broadening vs. Tb content. (a): the ^{89}Y-static signal, (b): the ^{27}Al-MAS signal of Al(6).

same relation between the brightness and the distribution of Tb^{3+} ions was obtained in the red phosphor, Eu-Y_2O_3.[1] Red phosphor, Eu-Y_2O_2S showed a similar relation as well.[23] This correlation between the brightness and the distribution of Tb^{3+} ions seemed to be a common characteristic in both green and red phosphors.

Conclusions

In this paper we characterized Tb-$Y_3Al_5O_{12}$ phosphors on the basis of the effects via incorporated paramagnetic ions on the chemical shifts, the spin-lattice relaxation time, and the line-broadening of ^{89}Y-MAS and -static and ^{27}Al-MAS resonances. It was shown that the pseudocontact mechanisms via Tb^{3+} ions influence Y nuclei especially located within 1 nm of the Tb^{3+} ion, which were observed in ^{89}Y-MAS NMR spectroscopy. The shift of the newly appeared shoulder peaks in Tb doped $Y_3Al_5O_{12}$ were found to be predominantly caused by the pseudocontact mechanism via the second to fifth neighboring Tb^{3+} ions to the resonating ^{89}Y atom. Generally, if we analyze the intensities of such peaks with relation to the content of the paramagnetic rare-earth ion incorporated, the distribution of the rare-earth ions within the structure could be quantified. In the present case, unfortunately, the line-broadening by itself caused the poor resolution. Phosphor is a system where the distribution of the rare-earth ions is of importance for understanding the properties. Therefore, the analyses of the chemical shift, the spin-lattice relaxation times, and the line-broadening via rare-earth ions are so useful. In the present investigation it was made clear that the green phosphor with stronger brightness is produced by the homogeneous distribution of Tb^{3+} ions and that such samples shows broader linewidth. Generally, the highly homogeneous distribution of the paramagnetic ion is a key factor to obtain a phosphor with high brightness.

We wish to thank Miss Chisato Miura (Mitsubishi Chemical Co., Ltd.) for the preparation of compounds investigated.

References

1) T. Harazono, E. Yokota, H. Uchida, and T. Watanabe, *Bull. Chem. Soc. Jpn.*, **71**, 825 (1998).
2) T. Harazono and T. Watanabe, *Bull. Chem. Soc. Jpn.*, **70**, 2383 (1997).
3) A. R. Thompson and E. Oldfield, *J. Chem. Soc., Chem. Commun.*, **1987**, 27.
4) P. D. Battle, B. Montez, and E. Oldfield, *J. Chem. Soc., Chem. Commun.*, **1988**, 584.
5) R. Dupree and M. E. Smith, *Chem. Phys. Lett.*, **148**, 41 (1988).
6) A. A. Shemyakov and M. M. Savosta, *Fiz. Tverdogo Tela*, **35**, 236 (1993).
7) G. Balakrishnan, L. W. J. Caves, R. Dupree, D. M. Paul, and M. E. Smith, *Physica C*, **161**, 9 (1989).
8) Z. P. Han, R. Dupree, D. M. Paul, A. P. Howes, and L. W. J. Caves, *Physica C*, **181**, 355 (1991).
9) C. P. Grey, M. E. Smith, A. K. Cheethan, C. M. Dobson, and R. Dupree, *J. Am. Chem. Soc.*, **112**, 4670 (1990).
10) K. J. D. MacKenzie and R. H. Meinhold, *J. Mater. Chem.*, **4**, 1595 (1994).
11) "Handbook of Phosphors," ed by Phosphor Research Society, Ohm Co., Ltd., Tokyo (1987), p. 268.
12) T. Harazono, E. Yokota, H. Uchida, A. Hase, and C. Miura, "Yttrium Aluminate Phosphor," Japan Patent 120265, 1996.
13) F. S. Galasso, "International Series of Monographs in Solid State Physics, Vol. 7, Structure and Properties of Inorganic Solids," Pergamon Press Ltd. Pub., Oxford, (1970), p. 244.
14) W. F. van der Weg, Th. J. A. Popma, and A. T. Vink, *J. Appl. Phys.*, **57**, 5450 (1985).
15) D. Massiot, C. Bessada, J. P. Coutures, and F. Taulelle, *J. Magn. Reson.*, **90**, 231 (1990).
16) A. Emiraliev, A. G. Kocharov, R. V. Vakradze, I. Karimov, and Z. I. Akhmedzhanov, *Kristallografiya*, **21**, 211 (1976).
17) W. Zhonghua, L. Kunquan, D. Jun, L. Fenyu, F. Zhengmin, and F. Zhengzhi, *Z. Phys. B*, **82**, 15 (1991).
18) B. J. Bleaney, *J. Magn. Reson.*, **8**, 91 (1972).

19) T. Harazono, R. Adachi, and T. Watanabe, "Proceedings of the 36th NMR Symposium," Tokyo, October , 1997, Abstr., p. 67.
20) B. N. Figgis, "Introduction to Ligand Field," Wiley-Interscience, New York (1966).
21) J. H. Van Vleck, *Phys. Rev.*, **74**, 168 (1948).
22) A. Abragam, "Principles of Nuclear Magnetism," the Clarendon Press, Oxford (1961), Chap. 9.
23) T. Harazono et al., "Yttrium Oxisulfide Phosphor," Japan Patent 110166, 1998.
24) Specification of Colors according to the Commision Internationale de l'Eclairage (CIE) 1931. JIS handbook 33, "Colors" Z8701-1982, ed by Japan Society of Standard, p. 117.